AGU PUBLICATIONS

Global Biogeochemical Cycles

RESEARCH ARTICLE
10.1002/2017GB005643

Temperature and oxygen dependence of the remineralization of organic matter

C. Laufkötter[1], Jasmin G. John[2], Charles A. Stock[2], and John P. Dunne[2]

[1]Program in Atmospheric and Oceanic Sciences, Princeton University, Princeton, New Jersey, USA, [2]National Oceanic and Atmospheric Administration/Geophysical Fluid Dynamics Laboratory, Princeton, New Jersey, USA

Key Points:
- Remineralization of particulate organic matter depends on temperature (Q_{10} 1.5–2.01) and on oxygen (half-saturation constant 4–12 micromol/L)
- The temperature and oxygen dependence cause an additional 10% decrease in carbon flux at 500 m
- The temperature dependence decreases the volume of the oxygen minimum zone, reducing a ubiquitous bias in global biogeochemical simulations

Supporting Information:
- Supporting Information S1

Correspondence to:
C. Laufkötter,
cl17@princeton.edu

Citation:
Laufkötter, C., J. G. John, C. A. Stock, and J. P. Dunne (2017), Temperature and oxygen dependence of the remineralization of organic matter, *Global Biogeochem. Cycles*, *31*, 1038–1050, doi:10.1002/2017GB005643.

Received 15 FEB 2017
Accepted 31 MAY 2017
Accepted article online 6 JUN 2017
Published online 4 JUL 2017

Abstract Accurate representation of the remineralization of sinking organic matter is crucial for reliable projections of the marine carbon cycle. Both water temperature and oxygen concentration are thought to influence remineralization rates, but limited data constraints have caused disagreement concerning the degree of these influences. We analyze a compilation of particulate organic carbon (POC) flux measurements from 19 globally distributed sites. Our results indicate that the attenuation of the flux of particulate organic matter depends on temperature with a Q_{10} between 1.5 and 2.01, and on oxygen described by a half-saturation constant between 4 and 12 μmol/L. We assess the impact of the temperature and oxygen dependence in the biogeochemistry model Carbon, Ocean Biogeochemistry, and Lower Trophics, coupled to Geophysical Fluid Dynamics Laboratory's Earth System Model ESM2M. The new remineralization parameterization results in shallower remineralization in the low latitudes but deeper remineralization in the high latitudes, redistributing POC flux toward the poles. It also decreases the volume of the oxygen minimum zones, partly addressing a long-standing bias in global climate models. Extrapolating temperature-dependent remineralization rates to the surface (i.e., beyond the depth range of POC flux data) resulted in rapid recycling and excessive surface nutrients. Surface nutrients could be ameliorated by reducing near-surface rates in a manner consistent with bacterial colonization, suggesting the need for improved remineralization constraints within the euphotic zone. The temperature and oxygen dependence cause an additional 10% decrease in global POC flux at 500 m depth, but no significant change in global POC flux at 2000 m under the RCP8.5 future projection.

1. Introduction

Each year, 5–10 Pg organic carbon are exported into the ocean interior [*Schlitzer*, 2002; *Dunne et al.*, 2005; *Henson et al.*, 2011], caused by the combination of biological production of organic matter at the surface and subsequent sinking of particulate organic carbon (POC) (the biological pump) [*Volk and Hoffert*, 1985; *Passow and Carlson*, 2012]. During particle sinking, zooplankton and bacteria degrade and remineralize that sinking organic matter, thereby releasing inorganic carbon back into the water column. The remineralization depth, often defined as the depth at which 63% of the material has remineralized, is of particular importance as it determines the time interval until the carbon comes in contact with the atmosphere again. If remineralization shoals in response to climate change, it will lead to a release of carbon higher in the water column, which has been shown to substantially lower the ocean's capacity to draw down anthropogenic carbon from the atmosphere [*Kwon et al.*, 2009].

While POC flux generally attenuates with depth in a roughly exponential way, the exact shape of the exponential function varies between regions [*Berelson*, 2001]. Many drivers have been suggested to affect the shape of this "remineralization curve" by either affecting the sinking speed of the particles or the intensity of the remineralization. Plankton community structure and aggregation processes are assumed to alter particle sizes and densities, which affect the sinking speed and hence the remineralization curve [*Burd and Jackson*, 2009]. In particular, the inclusion of dense minerals such as silicate, calcium carbonate, and lithogenic material is assumed to either act as ballast and increase particle sinking speed or partly protect organic matter from remineralization [*Armstrong et al.*, 2002; *Klaas and Archer*, 2002].

Since oxic remineralization requires oxygen, low oxygen concentrations are expected to decrease remineralization rates. Indeed, significantly weaker attenuation of POC flux within oxygen minimum zones compared

to sites with higher oxygen concentration has been observed [*Devol and Hartnett*, 2001]. *Van Mooy et al.* [2002] performed incubation experiments using oxic and suboxic water, showing that under suboxic conditions a greater fraction of POC is resistant to degradation. *Andersson et al.* [2008] performed a study in the Arabian Sea showing that respiration of phytodetritus depends on oxygen. However, despite evidence for the oxygen dependence of remineralization, it is unclear how exactly it should be parameterized and to date only a few global biogeochemical models include an oxygen dependence in their parameterization of remineralization [*Laufkötter et al.*, 2016].

Temperature is assumed to influence remineralization rates, as the metabolic processes of bacteria and zooplankton which are responsible for the remineralization are temperature dependent [*López-Urrutia et al.*, 2006]. Laboratory studies show that the carbon-specific respiration rate when degrading diatom aggregates increases strongly with temperature [*Iversen and Ploug*, 2013]. However, temperature effects on remineralization have not yet been directly observed in the field. It is therefore unclear whether remineralization rates are strongly driven by temperature in the open ocean or if the temperature effect is masked by other processes. For instance, increases in temperature will decrease the viscosity of water, which would allow for faster sinking of particles and might balance out or at least diminish temperature effects on remineralization [*Taucher et al.*, 2014]. To date, the strongest evidence for a temperature effect in the field comes from a study from *Marsay et al.* [2015], who show a correlation between the remineralization length scale and the average upper 500 m water temperature for eight sites.

Because of the uncertainty in parameterization of remineralization, current Earth System Models either implement a temperature-independent remineralization (e.g., the HadGEM model family) [*HadGEM Team et al.*, 2011] or assume a temperature-dependent remineralization with a Q_{10} value similar to what is used for phytoplankton growth (e.g., the IPSL-PISCES model) [*Aumont et al.*, 2015]. Even though the oxygen dependence of remineralization is more established, only a few models currently implement this relationship, e.g., *Dunne et al.* [2013] and *Aumont et al.* [2015]. These differences in the parameterization of remineralization are partly responsible for the large uncertainty in future projections of the biological pump [*Laufkötter et al.*, 2016]. Still, the impact of a temperature- and oxygen-dependent remineralization on the carbon cycle has not yet been systematically examined in a coupled carbon-climate Earth System Model.

Here we present constraints for a temperature and oxygen dependence of the attenuation of the POC flux. We conduct a statistical analysis to identify maximum likelihood values for oxygen and temperature constraints, using a compilation of POC flux measurements from 19 globally distributed sites covering a broad range of ocean conditions. We then assess the impact on remineralization and related biogeochemical patterns separately, and in combination, within the global biogeochemistry model COBALT, coupled to Geophysical Fluid Dynamics Laboratory's (GFDL's) Earth System Model ESM2M.

2. Methods

2.1. Data

We use measurements of POC flux, ballast minerals (opal, $CaCO_3$, and lithogenic material), temperature, and oxygen concentration that have been published between 1987 and 2015. We include all publicly available POC flux data where the POC flux was measured at multiple depths throughout the twilight zone. Overall, these criteria left us with 206 data points from 19 different sites. An overview of the sites, including their (geographic) coordinates and their reference, is given in Table 1 and in Figure 1. Three of the sites (6, 9, and 18) are on top of oxygen minimum zones with oxygen values below 10 μmol/L. For temperature, the sites cover subtropical and tropical water (e.g., stations 4, 12, and 17) as well as temperate and polar water (e.g., stations 2, 3, 14, 15, and 19). Depending on the site, POC flux has been measured with either surface- or bottom-tethered sediment traps or neutrally bouyant sediment traps. For the measurements within/below the mixed layer (80–200 m depth) we use ^{234}Th-based estimates of POC flux in some cases.

We assume that a fraction of the POC is associated with ballast material and therefore has a longer remineralization length scale (either because of protection from remineralization or because of faster sinking) [*Armstrong et al.*, 2002; *Iversen and Robert*, 2015]. In 11 out of 19 stations we use measurements of ballast minerals to calculate the protected fraction, using the relationships proposed by *Klaas and Archer* [2002]. We use measurements of opal, $CaCO_3$, and lithogenic material. For the other stations no ballast data is available (see Table 1). For those stations we estimate that 7% of the flux at the base of the euphotic zone is associated with ballast material, based on the global average from *Dunne et al.* [2007]. Temperature and oxygen

Table 1. List of Stations, Their Geographical Location, Whether Temperature, O_2, and Ballast Data is Available and References

#	Name	Latitude	Longitude	T and O_2 data	Ballast	Reference
1	PAP	47.0°N	16.5°W	WOA	Yes	*Marsay et al.* [2015]
2	Irminger	60.8°N	31.6°W	WOA	Yes	*Marsay et al.* [2015]
3	Iceland	62.1°N	24.4°W	WOA	Yes	*Marsay et al.* [2015]
4	NASG	25.6–26.8°N	30.3–31.6°W	WOA	Yes	*Marsay et al.* [2015]
5	WA	46.1–52.9°N	124.2′–125.1°W	Measured	No	*Devol and Hartnett* [2001]
6	MEX	22.2–22.4°N	106.2–106.4°W	Measured	No	*Devol and Hartnett* [2001]
7	Vertex I	36.1°N	122.6°W	O_2 WOA, T m.	No	*Knauer et al.* [1984]; *Martin et al.* [1987]
8	Vertex II, III	15.7–18.0°N	107.5–108.0°W	O_2 WOA, T m.	No	*Knauer et al.* [1984]; *Martin et al.* [1987]
9	Peru	15.5S	75.9°W	Measured	No	*Martin et al.* [1987]
10	Vertex 2,4	35.0°N	128.2°W	Measured	No	*Knauer et al.* [1984]; *Martin et al.* [1987]
11a	Vertex5	28.0°N	155.0°W	Measured	No	*Knauer et al.* [1984]; *Martin et al.* [1987]
11b	HOT	22.7°N	158.0°W	Measured	No	*Karl et al.* [1996]
12	Cariaco	10.5°N	64.7°W	Measured	Yes	*Thunell et al.* [2000]
13	ALOHA	22.7°N	158.0°W	Measured	Yes	*Buesseler et al.* [2007]
14	K2	47.0°N	160.0°E	Measured	Yes	*Buesseler et al.* [2007]
15	PAPA	50.0°N	145.0°W	Measured	Yes	*Wong et al.* [1999]
16	BATS	31.7°N	46.2°W	Measured	No	*Lutz et al.* [2002]
17	EqPac	9°N–12°S	140.0°W	Measured	Yes	*Honjo et al.* [1995]
18	Arab	16–18°N	58–62°E	Measured	Yes	*Murray et al.* [1996]; *Honjo et al.* [1999]
19	ASPZ	57–63°S	170.0°W	Measured	Yes	*Honjo et al.* [2000]; *Dunne et al.* [2005]

measurements were available for most sites; in the other cases we used values from World Ocean Atlas 2013 [*Garcia et al.*, 2014].

2.2. Statistical Analysis

In order to get constraints on the temperature and oxygen dependence of the remineralization, we approximate the POC flux, F, at depth z in a recursive way. We start with the observed flux at 150 m depth:

$$F_{z=150\text{ m depth}} = \text{observed flux at 150 m depth} \quad (1)$$

If there is no measurement at 150 m depth we use the measurement from the closest available depth, sometimes averaging measurements from above and below. The biggest deviation from 150 m depth is at ASPZ (measurement from 100 m depth). Full information about the depths from which measurements where

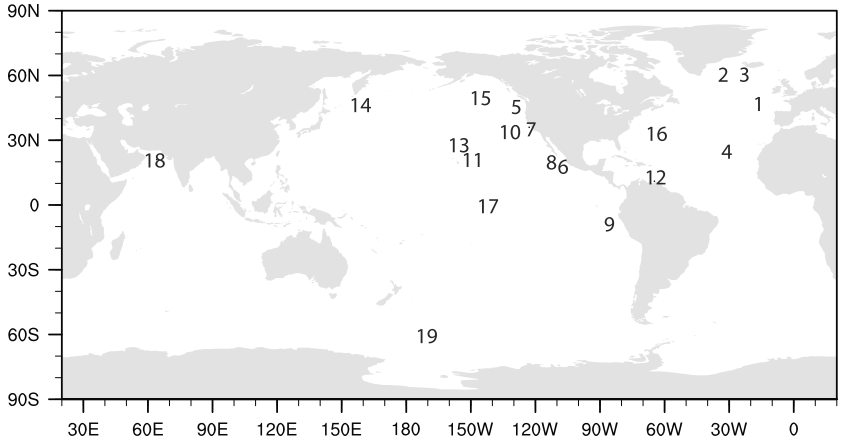

Figure 1. Geographic distribution of the measuring sites. Each number corresponds to a site; the sites are described in more detail in Table 1.

available can be found in the Supporting Information. We then calculate the flux stepwise for all depths z_i below 150 m where we have temperature and oxygen measurements, using the following function:

$$F_{z_i} = F_{\text{protected}} + F_{\text{free},z_{i-1}} \times e^{-\gamma \times e^{kT(z_{i-1})} \times \frac{O_2(z_{i-1})}{O_2(z_{i-1})+K_{O_2}} \times (z_i - z_{i-1})} \quad (2)$$

$F_{\text{protected}}$ is the fraction of the POC flux that is associated with opal, $CaCO_3$, and lithogenic material and is assumed to be protected from remineralization, either because of fast sinking or because of an actual protection from remineralization. The remaining part of the flux (F_{free}) is remineralized according to an exponential decay function, where γ is a basic remineralization rate, k is a coefficient describing the temperature dependence, T is temperature, and K_{O_2} a half-saturation constant describing the dependence on oxygen concentrations. We use a exponential dependence on temperature, as this has been shown to describe the temperature dependence of metabolic rates of bacteria. For oxygen, we assume a Michaelis-Menten-type relationship such that respiration rapidly declines at low values, but oxygen has only small effects on remineralization at higher values. The vertical resolution of the temperature and oxygen measurements is different between sites, but the average resolution is every 100 m. To obtain the optimal values for γ, k, and K_{O_2}, we minimize the error between the observations and the fitted values using the following error metric:

$$\text{error} = \sqrt{\frac{\sum |\log(\text{obs}) - \log(\text{fit})|^2}{n}} \quad (3)$$

We choose a logarithmic error metric to give equal weight to differences in particle fluxes across orders of magnitude. To quantitatively compare the extent to which remineralization models with and without temperature or oxygen dependence can explain patterns across the 19 sites (shown in Figure 1), we carry out three experiments:

1. Only temperature dependence by setting the oxygen parameter K_{O_2} to zero such that the oxygen term in equation (2) is one
2. Only oxygen dependence by setting the temperature parameter k to zero such that the temperature term in equation (2) is one
3. Both a temperature and oxygen dependence

For each of the three experiments, we find the best global parameters by minimizing the error between observations and fit at all sites simultaneously.

Given the sparse amount of data, the uncertainty in the POC flux measurements and a considerable scatter in the data at several sites, the best global parameters are an approximation of the actual temperature and oxygen dependence. In order to constrain the uncertainty stemming from the sparsity of data, we apply a χ^2 test to a range of parameter values to estimate the likelihood that a given set of parameters represents the actual temperature/oxygen dependence. We test temperature dependence parameters, k, from 0 (=no temperature dependence) to 0.09 (equivalent to a Q_{10} value of 2.45) paired with oxygen parameters, K_{O_2} ranging from 0 μmol/L (=no oxygen dependence) to 15 μmol/L. For each pair of temperature and oxygen parameters we use the value for the base respiration rate γ out of (0.003, … ,0.007) that optimizes the fit to the observations. The range of potential values for gamma is chosen such that the algorithm can choose between values corresponding to very shallow and very deep remineralization and the optimal solution therefore falls within the interval.

3. Parameter for Temperature and Oxygen Dependence

In the following we illustrate the impact of variations in temperature and oxygen concentration on the remineralization function in Figure 2, which shows the three remineralization functions described in section 2.2 for a subset of the sites. Each panel shows the measurements of the POC flux of a specific site, normalized to the flux at 150 m (black circles), and three lines representing the result of the three experiments for the respective site. The red line depicts the experiment with temperature forcing only, the blue line represents oxygen forcing only, and the green line shows both temperature and oxygen forcing. As a baseline comparison we also include the Martin curve [*Martin et al.*, 1987], using a globally constant b value of −0.858 (black). We show 9 of the 19 sites in Figure 2 and give a statistical comparison of all sites in Table 2. The plots for all 19 sites can be found in the supporting information. The supporting information also includes a table showing the error between fit and observations for each site individually.

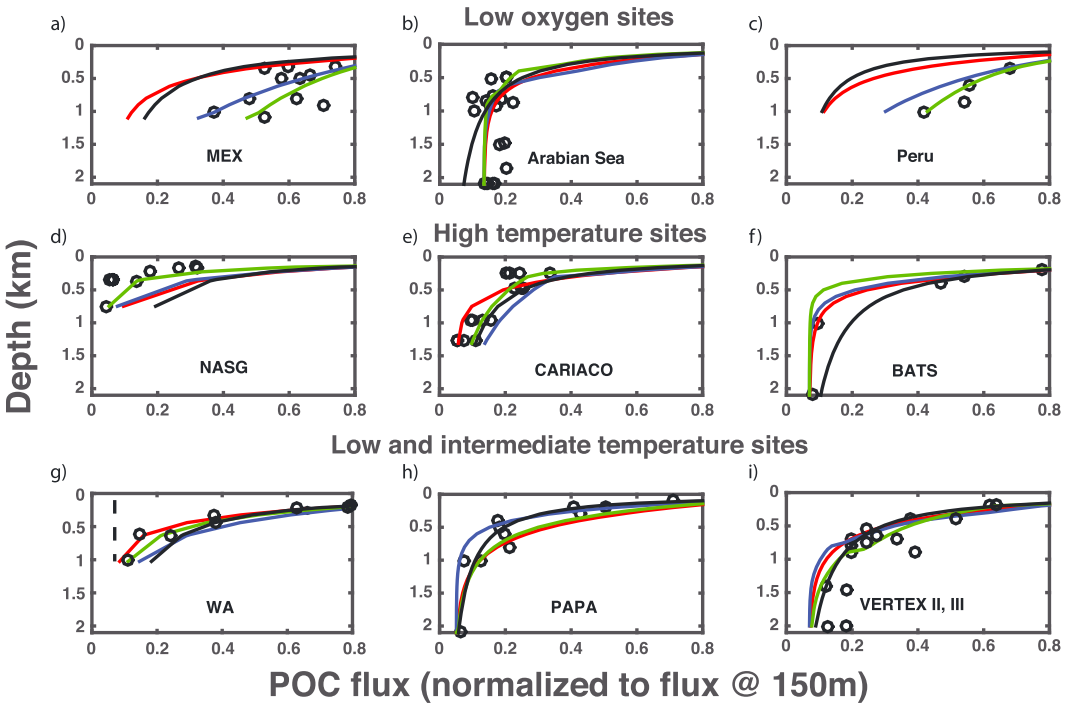

Figure 2. Illustrative examples of the fit of the exponential functions with temperature dependence only (red), oxygen dependence only (blue), temperature and oxygen dependence (green), and Martin curve (black) to observations from selected sites (black circles). (a–c) Data from sites with low deep ocean oxygen concentration; (d–f) data from sites with high deep ocean temperatures; and (g–i) data from sites from intermediate to cold temperature sites.

To illustrate the impact of the oxygen effect on remineralization, we show data from three sites which sample oxygen minimum zones where oxygen levels reach below 10 µmol/L (Figures 2a–2c show data from Peru, the Mexican Margin, and the Arabian Sea). At these sites the oxygen effect has the biggest impact (the difference between the red and the green line, i.e., temperature only and temperature and oxygen forcing, is particularly pronounced). The average error of the green line (T and O_2 forcing) is 0.27 at these three sites, compared to 0.61 for the red line (temperature forcing only). Particularly, in Peru and at the Mexican Margin, the experiments that include an oxygen dependence (blue and green lines) fit the data more closely than experiments without oxygen dependence.

To illustrate the impact of temperatures on remineralization, we aggregate the subtropical/tropical sites where the surface ocean is warmer than 20°C and the water is warmer than 10°C above 350 m depth (examples are NASG, Cariaco, and BATS; Figures 2d–2f) from the subpolar sites where the water temperature is below 7°C below 150 m depth (shown are WA and PAPA; Figures 2g and 2h. Again, the green line denoting the experiment with temperature and oxygen forcing is a better fit to the observations than the Martin curve (black line), O_2 forcing (blue line), or temperature forcing (red line) alone. The average error of the green line is 0.39, an almost 15% improvement over the blue line (error: 0.48) that has no temperature forcing. At the cold sites the temperature effect is less pronounced and the improvement by using a temperature forcing seems only small. However, our data set does include only a few subpolar/polar sites where POC flux measurements from different depths are available, hindering the demonstration of a temperature effect. Figure 2i shows data

Table 2. Comparison of Error Between Fit and Observations for All Sites[a]

	Martin Curve	T Forced	O_2 Forced	$T + O_2$ Forced
Error	0.4981	0.4824	0.4483	0.3944
% Improvement (compared to Martin Curve)		3	10	21

[a]The error metric is the RMSE between the logarithm of the normalized observations and the fit, as described in equation (3).

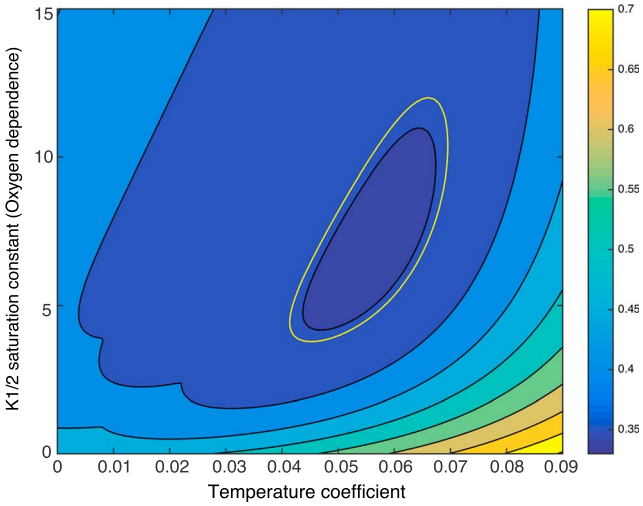

Figure 3. Error of different temperature and O_2 parameter sets and 95% confidence interval according to χ^2 test (region surrounded by white contour).

from one of the Vertex sites where the Martin curve was developed. This panel illustrates that our flux estimates are close to the Martin curve at intermediate water temperatures and regular O_2 concentrations and therefore consistent with the Martin curve at the site at which the Martin curve was derived.

Table 2 gives a statistical comparison of all sites simultaneously. Using only a temperature forcing results in a small improvement of 3% compared to the Martin Curve, oxygen forcing alone improves the fit by 10%, and using both a temperature and an oxygen dependence improves the fit by 21% (Table 2).

While averaged over all sites the temperature and oxygen dependence do improve the fit significantly, there are also sites where the temperature and oxygen dependence worsen the fit (see Table S1). Considering the sparse amount of data, the uncertainty in the POC flux measurements and a considerable scatter in the data at several sites, our parameters are at best an approximation of the actual temperature and oxygen dependence. To constrain the uncertainty stemming from the sparsity of data, we apply a χ^2 test to a range of parameter values to estimate the likelihood that a given set of parameters represents the actual temperature/oxygen dependence. Figure 3 shows the error between all observations and the fit with temperature and oxygen dependence, using a range of temperature and oxygen parameters. Blue indicates a small error (equivalent to good fit) and yellow indicates higher errors (a less optimal fit). In addition, the figure shows the contour around the parameter pairs that are in the 95% confidence interval; i.e., the interval outside of which a parameter set can be rejected with 95% confidence according to the χ^2 test. Temperature coefficients smaller than 0.05 and larger than 0.075, as well as oxygen half-saturation constants smaller than 5 μmol L^{-1} and larger than 12 μmol L^{-1}, are outside of the 95% confidence interval. We therefore conclude that the attenuation of the POC flux can be best explained with a temperature parameter between 0.041 and 0.07 (equivalent to a Q_{10} value of 1.5–2.01) and an oxygen parameter between 4 and 12 μmol L^{-1}.

4. Earth System Simulations

In the following we examine the impact of the temperature and oxygen dependence on marine primary production, biogeochemistry, and the oceanic carbon uptake under climate change. To this end, we use the biogeochemistry model Carbon, Ocean Biogeochemistry, and Lower Trophics version 1.0 (COBALT) [*Stock et al.*, 2014], coupled to GFDL's global 3-D coupled carbon-climate Earth System Model ESM2 M [*Dunne et al.*, 2013]. COBALT has been extensively described and evaluated in *Stock et al.* [2014]. Here we restrict ourselves to a brief summary of the main components and a description of how particle sinking and remineralization is handled. COBALT implements three phytoplankton functional types, large, small phytoplankton, and diazotrophs. The large phytoplankton type represents diatoms if silicate concentration in the water is sufficiently high and nondiatom large phytoplankton (such as dinoflagellates and other large eukaryotes) otherwise. The small phytoplankton group comprises phytoplankton smaller than 10 μm aside from diazotrophs. Phytoplankton growth is limited by several nutrients (nitrate, ammonia, phosphate, and iron), light, and temperature. The phytoplankton is grazed by three zooplankton functional types, micro, medium, and large zooplankton. Large zooplankton are parameterized as large copepods and euphausids, medium zooplankton are parameterized as small to medium-bodied copepods, and microzooplankton represent all heterotrophic zooplankton smaller than 200 μm. Besides grazing, further phytoplankton loss terms are aggregation, exudation to dissolved organic material, and lysis by viruses. Calcite and aragonite are produced by a fraction of the small

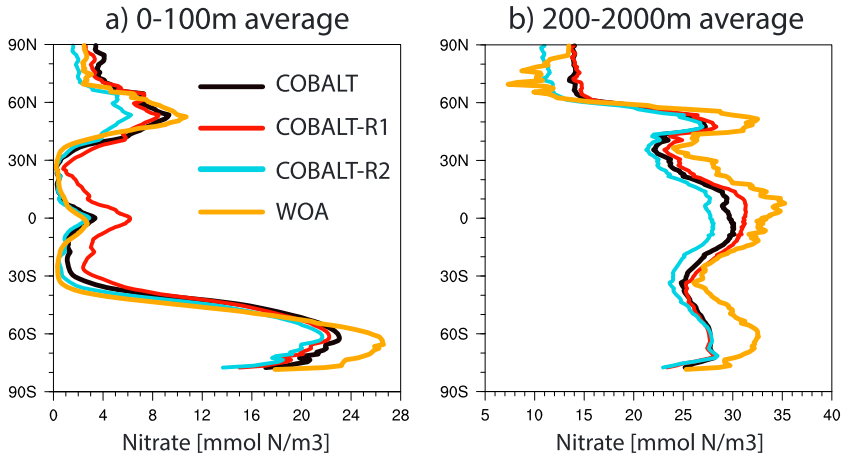

Figure 4. Zonal comparison of average (a) 0–100 m and (b) 200–2000 m depth nitrate concentration. The black line represents COBALT, red is COBALT-R1, cyan COBALT-R2, and orange the observations from the World Ocean Atlas.

phytoplankton (assumed to represent coccolithophores) and a fraction of zooplankton (i.e., foraminifera and pteropods). Sinking particles of organic matter are formed via grazing by medium and large zooplankton (fecal pellet production) and aggregation of small and large phytoplankton. A fraction of the organic material is assumed to be associated with ballast minerals (calcium carbonate, silicate, or lithogenic material) and sinks and remineralizes according to the length scales of the ballast materials. The remaining particles sink with a sinking speed of 100 m/day and are subject to remineralization which is described using an exponential decay function. Remineralization is independent from temperature but depends on oxygen described by a Michaelis-Menten function with a half-saturation constant of 20 μmol/L.

To examine the impact of the temperature and oxygen dependence on marine production and the oceanic carbon uptake under climate change, we update COBALT by adding a temperature dependence to the remineralization function and use the optimal values for γ, the temperature and oxygen parameter derived in section 3. We call this updated version of COBALT COBALT-R1.

The temperature-dependent remineralization rates included in COBALT-R1 can lead to very high remineralization rates in warm surface waters. The data used to constrain it, however, come from colder water below 150 m. Colonization of sinking material occurs throughout the euphotic zone, potentially reducing remineralization in the immediate vicinity of the ocean surface relative to R1 rates [*Mislan et al.*, 2014]. We thus considered a third model version (COBALT-R2) that decreases remineralization relative to COBALT-R1 toward the surface before ramping up remineralization rates to R1 values below 150 m. This decrease in remineralization is obtained by multiplying

$$\frac{z}{z + K_z}$$

to the remineralization function in COBALT-R1, where z = depth and $K_z = 50$ m.

4.1. Model Evaluation

We performed a spin-up of 1000 years with the original COBALT and additional 300 years with COBALT-R1 and COBALT-R2 until the drift in POC flux, oxygen, and nitrate in the twilight zone is negligible in each model version. After the spin-up, the models differed in the concentration of nutrients in surface and subsurface waters, the attenuation of the POC flux with depth and the extent of the oxygen minimum zones. Figure 4 compares the simulated nitrate concentration in all models at the surface and in the 200–2000 m depth with observations from the World Ocean Atlas (WOA) [*Garcia et al.*, 2014]. All models capture the general pattern with low values in the gyres and high values in upwelling regimes. In the surface low latitudes, however, COBALT-R1 has a positive bias of 2 mmol N/m^3. In contrast, all models underestimate the nutrient concentration in the deep ocean (200–2000m), but COBALT-R1 is closest to the WOA values. In the Southern Ocean, all three model versions slightly underestimate the nutrient concentrations at all depths. However, as the Southern Ocean is iron limited, we consider the representation of the low latitude nitrate concentration to be more important for simulations of marine primary and export production. Overall, COBALT-R1 has the highest correlation

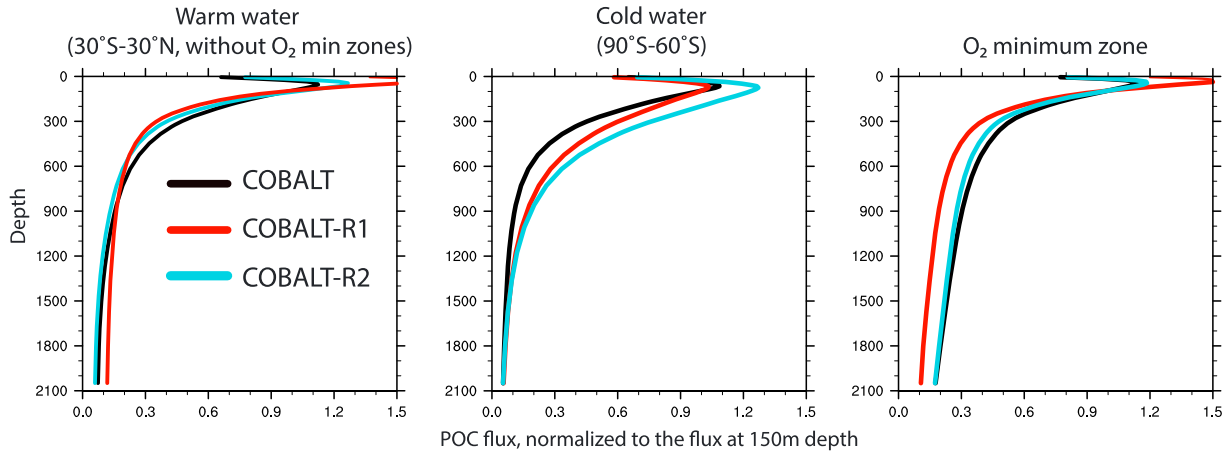

Figure 5. Model simulations of the remineralization curve in different temperature and oxygen regimes.

with WOA values (Spearman rank correlation of 0.93, while COBALT and COBALT-R2 both have correlations of 0.89) and the smallest RMSE (5.6 mmol m^{-3}, while the RMSE for COBALT and COBALT-R2 is 6.3 mmol m^{-3} and 6.8 mmol m^{-3}, respectively).

The shape of the remineralization curve for all three model versions and for different temperature and oxygen regimes are shown in Figure 5. The effect of the temperature dependence (included in COBALT-R1 and COBALT-R2, red, and blue lines, respectively) is most noticeable between 300 and 900 m depth, where it leads to a faster (shallower) attenuation of the POC flux in the warm low latitudes and slower (deeper) attenuation in the cold high latitudes. When comparing to our observations, COBALT-R1 matches the observations best; however, the differences between the models are small (average error: 0.57, 0.56, and 0.67, for COBALT, COBALT-R1, and COBALT-R2, respectively). As a consequence of the faster POC remineralization in warm water, the volume of the oxygen minimum zones is significantly smaller (and closer to observational estimates, Table 3) in COBALT-R1 as a larger amount of organic matter is remineralized higher in the water column due to the temperature dependence (Figure 5a). COBALT-R2 has a higher annual export production at 100 m depth (8 Gt C/year) than COBALT and COBALT-R1 (6.5 and 6.3 Gt C/year, respectively); therefore, despite the temperature dependence the amount of POC that is remineralized in the intermediate water column in the low latitudes is similar to COBALT. As a result, COBALT-R2 and COBALT simulate equally large oxygen minimum zones (Table 3). Overall, while COBALT-R2 simulates the most realistic surface nitrate concentrations, COBALT-R1 matches the observations from our POC database best, significantly improves the representation of the oxygen minimum zones and is closest to the WOA data of deep ocean nitrate.

At 2000 m depth, the unprotected POC is largely remineralized in all model versions, the remaining POC remineralizes according to the remineralization rate of the associated ballast material. The only region where unprotected POC is left at 2000 m depth is the area below the oxygen minimum zones (Figure 5), as the oxygen dependence strongly diminishes remineralization in low oxygen water. Here a significant amount of unprotected POC remains in COBALT and COBALT-R2 and a smaller amount in COBALT-R1. As both COBALT and COBALT-R2 overestimate the volume of the oxygen minimum zones, the POC flux under the oxygen minimum zones is likely overestimated as well.

Table 3. Comparison of the Simulated Volume of Suboxic Water (in 10^6 km^3) in COBALT, COBALT-R1, and COBALT-R2 With Observational Estimates From *Bianchi et al.* [2012]

Model	<20 mmol O_2/m^3	<5 mmol O_2/m^3
COBALT	94.3	27.1
COBALT-R1	40.8	7.1
COBALT-R2	89.4	28.4
CMIP5 models [*Bopp et al.*, 2013]	-	0.4–51.4, average 25.7
Estimate by *Bianchi et al.* [2012]	12.9	1.05

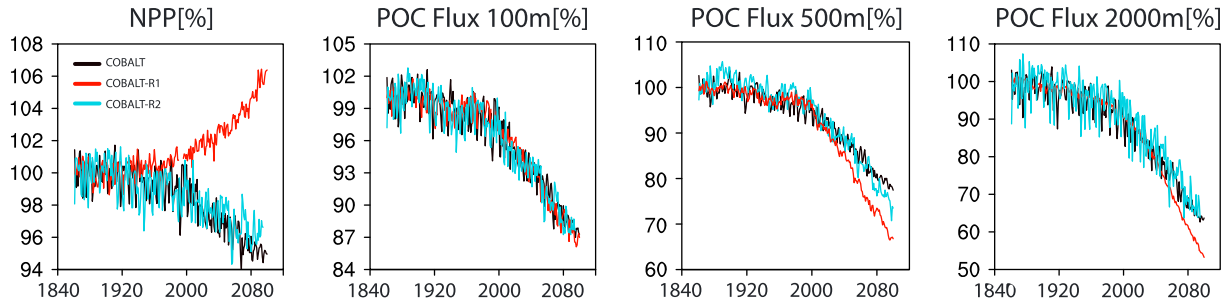

Figure 6. Model projections of global NPP and the global POC flux at 100, 500, and 2000 m depth. The changes are shown in percent; we define the average of the first 20 years as 100%. Note that the *y* axis differs between the plots.

COBALT-R1 also has a larger protected fraction in the low latitudes compared to the other model versions, resulting in a slightly larger POC flux at 2000 m. This is caused by the higher nutrient concentration due to rapid recycling in the surface ocean, which allows for stronger calcite and aragonite production in the surface plankton community (not shown). However, given that the surface nutrient concentration in COBALT-R1 has a positive bias (Figure 4), the lower protected flux in the other two model versions might be more realistic.

4.2. Future Projections

Figure 6 shows projections of net primary production (NPP), POC flux at 100 m, at 500 m, and at 2000 m depth under RCP8.5, as simulated by the three COBALT versions. In terms of NPP, the original COBALT code suggests decreases by 6% between 1840 and 2100. In contrast, COBALT-R1 projects an increase of similar magnitude. This increase is driven by both accelerated phytoplankton growth and faster remineralization of nutrients in response to global warming. However, the positive bias in contemporary surface nutrient concentrations means that nutrient limitation is too weak in COBALT-R1, such that the expected exacerbation of nutrient limitation with increasing stratification at low and midlatitudes under climate change [*Bopp et al.*, 2013; *Laufkötter et al.*, 2015] does not manifest. COBALT-R2, which has more realistic surface nutrients (Figure 4), simulates a decrease in NPP, albeit the decrease is slightly dampened compared to COBALT.

While the stronger remineralization supports high NPP in COBALT-R1, it also strongly attenuates the POC flux such that at 100 m depth all three model versions agree on decreases in POC flux of 13% between 1840 and 2100. At 500 m depth, where the temperature dependence caused the strongest differences between the models, COBALT suggests decreases by 20% while COBALT-R1 projects decreases by 30%. In COBALT-R2 the 500 m depth POC flux decreases by 25%. The reason for the weaker decrease in COBALT-R2 is that it has a significantly larger oxygen minimum zone, within which remineralization changes only slightly, dampening the global decrease in POC flux. When excluding the oxygen minimum zone, COBALT-R2 projects similar decreases like COBALT-R1.

At 2000 m depth, COBALT and COBALT-R2 suggest decreases of 35% until 2100. This trend is intensified in COBALT-R1 to a decrease of 45%. However, the stronger decrease in COBALT-R1 is not a direct consequence of the temperature dependence but rather a consequence of both the more realistic volume of suboxic water and differences in the surface ocean plankton community. All models project little changes in POC flux below the oxygen minimum zones. As the oxygen minimum zone is significantly smaller in COBALT-R1, a much larger area remains in which the POC flux decreases like in the remaining low latitudes. In addition, COBALT-R1 has a larger initial calcite and aragonite production in the surface plankton community (not shown) caused by the positive bias in surface nutrients. This $CaCO_3$ production reduces during climate change, leading to an additional decrease in POC flux at 2000 m depth. The decrease in POC flux at 2000 m co-occurs with a decrease in oceanic carbon uptake of 0.4 PgC/year in COBALT-R1 compared to COBALT and COBALT-R2.

5. Discussion

The data analysis in this work represents the strongest evidence to date for a global temperature dependence of the attenuation of the POC flux in the open ocean. The range of Q_{10} values to which we could constrain the temperature parameter are close to values used for phytoplankton growth and bacteria (typically between 1.5 and 2.2) [*Eppley*, 1972; *White et al.*, 1991; *Bissinger et al.*, 2008; *Sherman et al.*, 2016]. Our results confirm

and extend attempts from previous authors to estimate the relationship between temperature and remineralization using a variety of approaches. *Marsay et al.* [2015] find a correlation between the remineralization length scale and the average upper 500 m water temperature, using average values from eight different stations. *McDonnell et al.* [2015] observe significantly higher remineralization rates in the warm subtropical gyres compared to respiration rates close to Antarctica, detected with RESPIRE sediment traps. *Weber et al.* [2016] reconstruct the POC flux on the basis of the deep ocean nutrient concentration in a data-constrained circulation model, their results support a temperature influence on remineralization. Finally, our results are also consistent with evidence of faster bacterial remineralization in warmer oceans in the Eocene epoch [*John et al.*, 2014].

However, despite the growing evidence for a relationship between temperature and particle flux attenuation, considerable uncertainty remains. The main obstacle is the uncertainty introduced by the use of different measuring techniques [*Buesseler et al.*, 2000] and the general sparsity of data. To get enough data points for our analysis, we combined measurements from different years and seasons and treated the resulting data set as a representative of the annual mean. As very little is known about seasonal and interannual variability in POC flux [*Henson et al.*, 2015] the additional uncertainty that stems from combining the measurements is barely quantified. Depth-resolved observations of the POC flux that capture the seasonal cycle and the interannual variability at key stations would help quantifying that uncertainty and improve our understanding of the POC flux. Additionally, observations of the POC flux contrasting particularly warm and cold sites would help to further narrow down the parameter range found in our study.

Also, we cannot discern from our method whether the relationship between water temperature and particle flux attenuation is driven by faster bacterial degradation and remineralization, by viscosity-induced differences in sinking speed or by indirect temperature effects such as differences in particle composition and/or plankton community structure in different temperature regimes. Faster remineralization in response to warming seems likely, given that increases in remineralization in response to temperature have been measured in the laboratory [*Iversen and Ploug*, 2013] and the effective Q_{10} values are consistent with the biological responses of phytoplankton and bacteria. Particle sinking rates showed no clear difference between warm and cold locations during the VERTIGO project [*Trull et al.*, 2008]; however, more recent observations indicate significantly faster sinking rates in cold water [*McDonnell et al.*, 2015]. The plankton community structure is also influenced by temperature and is likely to influence particle export [*Guidi et al.*, 2016], but understanding is just beginning to evolve, and it is not yet clear how exactly temperature affects particle composition. Our results summarize the net effect of temperature on particle flux attenuation and as such can be used to estimate an overall response of the POC flux to temperature changes. We would like to emphasize here that a better mechanistic understanding of processes in the twilight zone would increase our confidence in how the relationships identified in this work apply to future oceans.

5.1. Discussion of the Model Projections

The temperature dependence of remineralization is often listed among the key uncertainties in the biological pump [e.g., *Passow and Carlson*, 2012] and has been identified as a major difference in the parameterization of export production and POC flux in marine biogeochemistry models [*Laufkötter et al.*, 2016]. Our results suggest that the direct influence of the temperature effect on the POC flux is significant at 500 m depth but rather small at 2000 m depth. In addition, the temperature dependence plays an important role for the oxygen distribution in the ocean.

In terms of future NPP, our two model versions with temperature-dependent remineralization provide contradicting results. On the one hand, we find increases in future NPP in COBALT-R1, which appear to be driven by a temperature-induced acceleration of remineralization. This would be in line with a study from *Taucher and Oschlies* [2011], who report increases in global NPP under the Special Report on Emissions Scenarios A2 scenario in a temperature-dependent model configuration (Q_{10} value of 1.88) while NPP decreases in a temperature-independent configuration. However, instead of being caused by the temperature-dependent remineralization, the increase in NPP in COBALT-R1 might also be caused by the positive surface nutrient bias, such that phytoplankton is only weakly nutrient limited and a reduction in surface nutrients caused by global warming has only a moderate impact. Also, most CMIP5 models, including models that parameterize a temperature-dependent remineralization, project decreases in NPP [*Bopp et al.*, 2013].

On the other hand, COBALT-R2 projects decreases in NPP which are only slightly dampened compared to the projection of the temperature-independent model COBALT. In COBALT-R2, remineralization is reduced

toward the surface to reflect gradual colonization by bacteria with depth, resulting in surface nutrient concentrations very close to observations. However, as the measurements in our POC flux data set stem from below 100 m depth, we cannot determine the degree to which this remineralization curve resembles the remineralization curve in the real ocean. A better mechanistic understanding of the processes that form and remineralize particles in the upper ocean will be indispensable for a better understanding of the NPP response to climate change.

While projections of NPP appear to be rather sensitive to assumptions about temperature dependence, all our model projections of POC flux as well as the model studies by *Taucher and Oschlies* [2011] and *Segschneider and Bendtsen* [2013] indicate that the POC flux at 100 m depth does not react strongly to increases in temperature, even despite simulated increases in NPP. This points toward a strong coupling between the POC flux at 100 m and the upwelling of nutrients to the surface and consequentially indicates that the change in future POC flux at 100 m is mostly controlled by changes in physically driven vertical exchanges. In terms of deep ocean POC flux, we show that the strongest effect of the temperature dependance manifests at 500 m depth, where the differences between the temperature-dependent and temperature-independent models are largest. As a result, the transfer efficiency at 1000 m depth, which is the fraction of the POC flux at 100 m that reaches 1000 m depth, shows a clear latitudinal pattern with higher values in the high latitudes and low values in the subtropical gyres. In addition, the oxygen dependence leads to intermediate values of transfer efficiency below the tropical oxygen minimum zones. Taken together, this pattern of transfer efficiency is in high agreement with results from *Weber et al.* [2016], who reconstruct the POC flux on the basis of the deep ocean nutrient concentration in a data-constrained circulation model. *Henson et al.* [2015] define the transfer efficiency as the fraction of 100 m POC flux that reaches 2000 m depth. They report the opposite pattern with high values of transfer efficiency in the low latitudes and low values at high latitudes. At 2000 m depth, the POC flux in our model is mainly controlled by the ballasting material and the transfer efficiency at 2000 m shows only very small variations.

With respect to future changes in POC flux, the POC flux at 500 m depth in the temperature-dependent model versions decreases about 10% stronger than in the temperature-independent version until 2100. However, at 2000 m depth the POC flux barely responds to a temperature dependance of remineralization. The main reason is that in our model the flux at 2000 m depth is to a large extend controlled by the amount of ballast material, and the remineralization of ballast material is implemented equally in all three model versions. In addition, the water temperature changes only slightly in the 1000–2000 m depth layer (<0.4°C on average) so the strength of the remineralization changes only slightly. In contrast, the oxygen dependence and the extend of the oxygen minimum zone strongly influences the POC flux at 2000 m. Our results indicate that the overestimation of the oxygen minimum zone leads to a significant underestimation of the decrease in POC flux at 2000 m in our model.

6. Summary and Conclusion

In this work we show that variations in the attenuation of the flux or particulate organic carbon can be predicted using water temperature and oxygen concentration. We develop observation-based estimates for global parameter of these dependencies. According to our results, the attenuation of POC flux depends on temperature with a Q_{10} value between 1.5 and 2.01, and on oxygen with a half-saturation constant between 4 and 12 μmol/L, assuming an average sinking speed of 100 m/day. The temperature dependence of remineralization has been identified as a key difference in model parameterizations and is often assumed to cause uncertainty in projections of the marine carbon flux and might even lead to increases in net primary production (NPP). According to our results, increasing future NPP in response to temperature-dependent remineralization only occurs when nutrients are unrealistically high. With realistic surface nutrients, the temperature dependence has only a small impact on NPP projections. In addition, we show that temperature significantly influences the attenuation of the POC flux in the twilight zone (around 500 m depth) but has only a small effect at 2000 m depth. As there are currently large differences in how particle formation and sinking is implemented in models, a temperature effect might have different consequences in other models, particularly in models that do not use ballasting but different particle size classes. Besides impacts on the carbon cycle, the effects of the temperature dependence on oxygen distribution in the water column is of high relevance in our model as it influences the volume of the oxygen minimum zones, which in turn influence the response of the carbon cycle to global warming. A missing temperature dependence likely contributes

to the overestimation of the oxygen minimum zones in most current ocean biogeochemistry models. Finally, while we used only the optimal parameter set, further studies could test the uncertainty in model response caused by the range of likely temperature and oxygen parameters, as well as the response of the carbon cycle after 2100 when the warming reaches deeper ocean layers.

Acknowledgments
This research was supported by NOAA's Marine Ecosystem Tipping Points Initiative. We also thank the JGOFS SMP database (http://usjgofs.whoi.edu/mzweb/syndata.html) for hosting the *Honjo et al.* [2008] data.

References

Andersson, J. H., C. Woulds, M. Schwartz, G. L. Cowie, L. A. Levin, K. Soetaert, and J. J. Middelburg (2008), Short-term fate of phytodetritus in sediments across the Arabian Sea Oxygen Minimum Zone, *Biogeosciences*, *5*, 43–53, doi:10.5194/bg-5-43-2008.

Armstrong, R., C. Lee, J. Hedges, S. Honjo, and S. Wakeham (2002), A new, mechanistic model for organic carbon fluxes in the ocean based on the quantitative association of POC with ballast minerals, *Deep Sea Res., Part II*, *49*(1–3), 219–236, doi:10.1016/S0967-0645(01)00101-1.

Aumont, O., C. Ethé, A. Tagliabue, L. Bopp, and M. Gehlen (2015), PISCES-v2: An ocean biogeochemical model for carbon and ecosystem studies, *Geosci. Model Dev.*, *8*(8), 2465–2513, doi:10.5194/gmd-8-2465-2015.

Berelson, W. M. (2001), The flux of particulate organic carbon into the ocean interior: A comparison of four US JGOFS regional studies, *Oceanography*, *14*(4), 59–67.

Bianchi, D., J. P. Dunne, J. L. Sarmiento, and E. D. Galbraith (2012), Data-based estimates of suboxia, denitrification, and N_2O production in the ocean and their sensitivities to dissolved O_2, *Global Biogeochem. Cycles*, *26*, GB2009, doi:10.1029/2011GB004209.

Bissinger, J. E., D. J. S. Montagnes, J. Sharples, and D. Atkinson (2008), Predicting marine phytoplankton maximum growth rates from temperature: Improving on the Eppley curve using quantile regression, *Limnol. Oceanogr.*, *53*(2), 487–493, doi:10.4319/lo.2008.53.2.0487.

Bopp, L., et al. (2013), Multiple stressors of ocean ecosystems in the 21st century: Projections with CMIP5 models, *Biogeosciences*, *10*(10), 6225–6245, doi:10.5194/bg-10-6225-2013.

Buesseler, K. O., D. K. Steinberg, A. F. Michaels, R. J. Johnson, J. E. Andrews, J. R. Valdes, and J. F. Price (2000), A comparison of the quantity and composition of material caught in a neutrally buoyant versus surface-tethered sediment trap, *Deep Sea Res., Part I*, *47*, 277–294.

Buesseler, K. O., et al. (2007), Revisiting carbon flux through the ocean's twilight zone, *Science*, *316*(5824), 567–570, doi:10.1126/science.1137959.

Burd, A. B., and G. A. Jackson (2009), Particle aggregation, *Annu. Rev. Mar. Sci.*, *1*(1), 65–90, doi:10.1146/annurev.marine.010908.163904.

Devol, A. H., and H. E. Hartnett (2001), Role of the oxygen-deficient zone in transfer of organic carbon to the deep ocean, *Limnol. Oceanogr.*, *46*(7), 1684–1690, doi:10.4319/lo.2001.46.7.1684.

Dunne, J. P., R. A. Armstrong, A. Gnanadesikan, and J. L. Sarmiento (2005), Empirical and mechanistic models for the particle export ratio, *Global Biogeochem. Cycles*, *19*, GB4026, doi:10.1029/2004GB002390.

Dunne, J. P., J. L. Sarmiento, and A. Gnanadesikan (2007), A synthesis of global particle export from the surface ocean and cycling through the ocean interior and on the seafloor, *Global Biogeochem. Cycles*, *21*, GB4006, doi:10.1029/2006GB002907.

Dunne, J. P., et al. (2013), GFDL's ESM2 global coupled climate-carbon earth system models. Part II: Carbon system formulation and baseline simulation characteristics, *J. Clim.*, *26*(7), 2247–2267, doi:10.1175/JCLI-D-12-00150.1.

Eppley, R. (1972), Temperature and phytoplankton growth in the sea, *Fishery Bull.*, *70*(4), 1063–1085.

Garcia, H. E., R. A. Locarnini, T. P. Boyer, J. I. Antonov, O. K. Baranova, M. M. Zweng, J. R. Reagan, and D. R. Johnson (2014), *World Ocean Atlas 2013, Volume 4: Dissolved Inorganic Nutrients (Phosphate, Nitrate, Silicate)*, edited by S. Levitus and A. Mishonov, 25 pp., NOAA Atlas NESDIS 76.

Guidi, L., et al. (2016), Plankton networks driving carbon export in the oligotrophic ocean, *Nature*, *532*(7600), 465–470, doi:10.1038/nature16942.

HadGEM Team, et al. (2011), The HadGEM2 family of met office unified model climate configurations, *Geosci. Model Dev.*, *4*(3), 723–757, doi:10.5194/gmd-4-723-2011.

Henson, S. A., R. Sanders, E. Madsen, P. J. Morris, F. Le Moigne, and G. D. Quartly (2011), A reduced estimate of the strength of the ocean's biological carbon pump, *Geophys. Res. Lett.*, *38*, L04606, doi:10.1029/2011GL046735.

Henson, S. A., A. Yool, and R. Sanders (2015), Variability in efficiency of particulate organic carbon export: A model study, *Global Biogeochem. Cycles*, *29*, 33–45, doi:10.1002/2014GB004965.

Honjo, S., J. Dymond, R. Collier, and S. J. Manganini (1995), Export production of particles to the interior of the equatorial Pacific Ocean during the 1992 EqPac experiment, *Deep Sea Res. Part II*, *42*(2–3), 831–870, doi:10.1016/0967-0645(95)00034-N.

Honjo, S., J. Dymond, W. Prell, and V. Ittekkot (1999), Monsoon-controlled export fluxes to the interior of the Arabian Sea, *Deep Sea Res., Part II*, *46*(1999), 1859–1902.

Honjo, S., R. Francois, S. Manganini, J. Dymond, and R. Collier (2000), Particle fluxes to the interior of the Southern Ocean in the Western Pacific sector along 170°W, *Deep Sea Res., Part II*, *47*(15–16), 3521–3548, doi:10.1016/S0967-0645(00)00077-1.

Honjo, S., S. J. Manganini, R. A. Krishfield, and R. Francois (2008), Particulate organic carbon fluxes to the ocean interior and factors controlling the biological pump: A synthesis of global sediment trap programs since 1983, *Prog. Oceanogr.*, *76*(3), 217–285, doi:10.1016/j.pocean.2007.11.003.

Iversen, M. H., and H. Ploug (2013), Temperature effects on carbon-specific respiration rate and sinking velocity of diatom aggregates—Potential implications for deep ocean export processes, *Biogeosciences*, *10*(6), 4073–4085, doi:10.5194/bg-10-4073-2013.

Iversen, M. H., and M. L. Robert (2015), Ballasting effects of smectite on aggregate formation and export from a natural plankton community, *Mar. Chem.*, *175*, 18–27, doi:10.1016/j.marchem.2015.04.009.

John, E. H., J. D. Wilson, P. N. Pearson, and A. Ridgwell (2014), Temperature-dependent remineralization and carbon cycling in the warm Eocene oceans, *Palaeogeogr. Palaeoclimatol. Palaeoecol.*, *413*, 158–166, doi:10.1016/j.palaeo.2014.05.019.

Karl, D. M., J. R. Christian, J. E. Dore, D. V. Hebel, R. M. Letelier, L. M. Tupas, and C. D. Winn (1996), Seasonal and interannual variability in primary production and particle flux at Station ALOHA, *Deep Sea Res., Part II*, *43*(2), 539–568.

Klaas, C., and D. E. Archer (2002), Association of sinking organic matter with various types of mineral ballast in the deep sea: Implications for the rain ratio, *Global Biogeochem. Cycles*, *16*(4), 1116, doi:10.1029/2001GB001765.

Knauer, G. A., D. M. Karl, J. H. Martin, and C. N. Hunter (1984), In situ effects of selected preservatives on total carbon, nitrogen and metals collected in sediment traps, *J. Mar. Res.*, *42*, 445–462.

Kwon, E. Y., F. Primeau, and J. L. Sarmiento (2009), The impact of remineralization depth on the air-sea carbon balance, *Nat. Geosci.*, *2*(9), 630–635, doi:10.1038/ngeo612.

Laufkötter, C., et al. (2015), Drivers and uncertainties of future global marine primary production in marine ecosystem models, *Biogeosci. Discuss.*, *12*(4), 3731–3824, doi:10.5194/bgd-12-3731-2015.

Laufkötter, C., M. Vogt, N. Gruber, L. Bopp, J. Dunne, J. Hauck, J. John, I. Lima, R. Seferian, and C. Volker (2016), Projected decreases in future marine export production: The role of the carbon flux through the upper ocean ecosystem, *Biogeosciences*, *12*(4), 3731–3824, doi:10.5194/bgd-12-3731-2015.

López-Urrutia, A., E. San Martin, R. P. Harris, and X. Irigoien (2006), Scaling the metabolic balance of the oceans, *Proc. Natl. Acad. Sci. U.S.A.*, *103*(23), 8739–8744, doi:10.1073/pnas.0601137103.

Lutz, M., R. Dunbar, and K. Caldeira (2002), Regional variability in the vertical flux of particulate organic carbon in the ocean interior, *Global Biogeochem. Cycles*, *16*(3), 1037, doi:10.1029/2000GB001383.

Marsay, C. M., R. J. Sanders, S. a. Henson, K. Pabortsava, E. P. Achterberg, and R. S. Lampitt (2015), Attenuation of sinking particulate organic carbon flux through the mesopelagic ocean, *Proc. Natl. Acad. Sci. U.S.A.*, *112*(4), 1089–1094, doi:10.1073/pnas.1415311112.

Martin, J. H., G. A. Knauer, D. M. Karl, and W. W. Broenkow (1987), VERTEX: Carbon cycling in the northeast Pacific, *Deep Sea Res., Part I*, *34*(2), 267–285, doi:10.1016/0198-0149(87)90086-0.

McDonnell, A. M., et al. (2015), The oceanographic toolbox for the collection of sinking and suspended marine particles, *Prog. Oceanogr.*, *133*, 17–31, doi:10.1016/j.pocean.2015.01.007.

Mislan, K. A. S., C. A. Stock, J. P. Dunne, and J. L. Sarmiento (2014), Group behavior among model bacteria influences particulate carbon remineralization depths, *J. Mar. Res.*, *72*, 183–218.

Murray, J. W., J. Young, J. Newton, J. Dunne, T. Chapin, B. Paul, and J. J. Mccarthys (1996), Export flux of particulate organic carbon from the central equatorial Pacific determined using a combined drifting trap- ^{234}Th approach, *Deep Sea Res., Part II*, *43*(6), 1095–132, doi:10.1016/0967-0645(96)00036-7.

Passow, U., and C. A. Carlson (2012), The biological pump in a high CO_2 world, *Mar. Ecol. Prog. Ser.*, *470*(2), 249–271, doi:10.3354/meps09985.

Schlitzer, R. (2002), Carbon export fluxes in the Southern Ocean: Results from inverse modeling and comparison with satellite-based estimates, *Deep Sea Res., Part II*, *49*(9–10), 1623–1644, doi:10.1016/S0967-0645(02)00004-8.

Segschneider, J., and J. Bendtsen (2013), Temperature-dependent remineralization in a warming ocean increases surface pCO_2 through changes in marine ecosystem composition, *Global Biogeochem. Cycles*, *27*, 1214–1225, doi:10.1002/2013GB004684.

Sherman, E., J. Keith Moore, F. Primeau, and D. Tanouye (2016), Temperature influence on phytoplankton community growth rates, *Global Biogeochem. Cycles*, *30*, 550–559, doi:10.1002/2015GB005272.

Stock, C. A., J. P. Dunne, and J. G. John (2014), Global-scale carbon and energy flows through the marine planktonic food web: An analysis with a coupled physical-biological model, *Prog. Oceanogr.*, *120*, 1–28, doi:10.1016/j.pocean.2013.07.001.

Taucher, J., and A. Oschlies (2011), Can we predict the direction of marine primary production change under global warming?, *Geophys. Res. Lett.*, *38*, L02603, doi:10.1029/2010GL045934.

Taucher, J., L. T. Bach, U. Riebesell, and A. Oschlies (2014), The viscosity effect on marine particle flux: A climate relevant feedback mechanism, *Global Biogeochem. Cycles*, *28*, 415–422, doi:10.1002/2013GB004678.

Thunell, R. C., R. Varela, M. Llano, J. Collister, F. Muller-Karger, and R. Bohrer (2000), Organic carbon fluxes, degradation, and accumulation in an anoxic basin: Sediment trap results from the Cariaco Basin, *Limnol. Oceanogr.*, *45*(2), 300–308, doi:10.4319/lo.2000.45.2.0300.

Trull, T., S. Bray, K. Buesseler, C. Lamborg, S. Manganini, C. Moy, and J. Valdes (2008), In situ measurement of mesopelagic particle sinking rates and the control of carbon transfer to the ocean interior during the Vertical Flux in the Global Ocean (VERTIGO) voyages in the North Pacific, *Deep Sea Res., Part II*, *55*, 1684–1695, doi:10.1126/science.1137959.

Van Mooy, B. A. S., R. G. Keil, and A. H. Devol (2002), Impact of suboxia on sinking particulate organic carbon: Enhanced carbon flux and preferential degradation of amino acids via denitrification, *Geochim. Cosmochim. Acta*, *66*(3), 457–465, doi:10.1016/S0016-7037(01)00787-6.

Volk, T., and M. Hoffert (1985), Ocean carbon pumps: Analysis of relative strengths and efficiencies in ocean-driven atmospheric CO_2 changes, in *The Carbon Cycle and Atmospheric CO_2: Natural Variations Archean to Present, Geophys. Monogr. Ser.*, vol. 32, edited by E. Sundquist and W. Broecker, pp. 99–110, AGU, Washington, D. C., doi:10.1029/GM032p0099.

Weber, T., J. A. Cram, S. W. Leung, T. Devries, C. Deutsch, and D. M. Karl (2016), Deep ocean nutrients imply large latitudinal variation in particle transfer efficiency, *Proc. Natl. Acad. Sci. U.S.A.*, *113*(31), 8606–8611, doi:10.1073/pnas.1604414113.

White, P. A., J. Kalff, J. B. Rasmussen, and J. M. Gasol (1991), The effect of temperature and algal biomass on bacterial production and specific growth rate in freshwater and marine habitats, *Microbial Ecol.*, *21*, 99–118, doi:10.1007/BF02539147.

Wong, C. S., F. A. Whitney, D. W. Crawford, K. Iseki, R. J. Matear, W. K. Johnson, J. S. Page, and D. Timothy (1999), Seasonal and interannual variability in particle fluxes of carbon, nitrogen and silicon from time series of sediment traps at Ocean Station P, 1982–1993: Relationship to changes in subarctic primary productivity, *Deep Sea Res., Part II*, *46*, 2735–2760.